International Journal of Solids and Structures
Volume 44, Issue 9, 1 May 2007, Pages 2943-2960
doi:10.1016/j.ijsolstr.2006.08.032

Analytical modeling of synthetic fiber ropes. Part II: A linear elastic model for 1 + 6 fibrous structures

Seyed Reza Ghoreishi[1], Peter Davies[2], Patrice Cartraud[1], Tanguy Messager[3]

1. Institut de recherche en Génie civil et Mécanique (GéM), Ecole Centrale de Nantes, BP92101, 44321 Nantes, France
2. IFREMER, Materials and Structures group BP70, 29280 Plouzané, France
3. Université de Nantes, Nantes Atlantique Universités, Institut de recherche en Génie civil et Mécanique (GéM), Ecole Centrale de Nantes, BP92101, 44321 Nantes , France

Corresponding author: Patrice CARTRAUD ; Ecole Centrale de Nantes ; BP 92101 ; 44321 Nantes cédex3 France ; Tel: +33.2.40.37.25.85 ; Fax: +33.2.40.37.25.73 ; Email: patrice.cartraud@ec-nantes.fr

Abstract:

In part I of this study it was shown that, to model synthetic fiber ropes, two scale transition models can be used in sequence. The first model (continuum model) has been presented in the part I and the present paper examines the behavior of a fibrous structure consisting of 6 helicoidal strands around a central core (1 + 6 structure). An analytical model will be presented which enables the global elastic behavior of such a cable under tension–torsion loading to be predicted. In this model, first, the core and the strands are described as Kirchhoff–Love beams and then the traction–torsion coupling behavior is taken into account for both of them. By modeling the contact conditions between the strands and the core, with certain assumptions, it is possible to describe the behavior of the cable section as a function of the degrees of freedom of the core. The behavior of the cable can thus be deduced from the tension–torsion coupling behavior of its constituents. Tensile tests have been performed on the core, the strands and then on a full scale 205 ton failure load cable. Finally, predicted stiffness from the analytical models is compared to the test results.

Keywords: Fiber rope; Simple strand; Wire; Aramid; Analytical model; Testing

1. Introduction

As presented in the part I (Ghoreishi et al., submitted to International Journal of Solids and Structures) of this work, large synthetic fiber ropes are characterized by a very complex architecture, and a hierarchical structure in which the base components (fiber or yarn) are transformed by a twisting operation. The resulting structure is then a base component for the next higher structure. Its hierarchical structure leads to the hierarchical approach where the top is the fiber rope and the bottom is the base components, with several different types of elements between the base component and the fiber rope. As indicated in part I of this work the fiber rope consists of two different types of structure: multilayered and 1+6 structures. It has been also shown that to go from fiber to rope, two scale transition models are necessary that are used in sequence. An analytical closed-form formulation (continuum model) of a multilayered structure has been developed in part I. The objective of the present paper is the modeling of the static behavior of a 1+6 fibrous structure subjected to axial loads, using the mechanical behavior of the core and strands, and the geometric description of the structure.

In section 2, the global behavior of the cable will be described and then, in section 3, an overview of the existing models for such structures will be given. In section 4, an extension of Labrosse's model to predict global response of a 1+6 fibrous rope structure, is developed. The analytical models are compared in section 5. Tensile tests, on two different fiber ropes, have been performed and provide the experimental data that are described in section 6. In section 7, results of analytical models are compared to experimental data.

2. Cable global behavior

Let us consider a 1+6 fiber rope made of six helical strands (wires) wrapped around a

straight core as illustrated in figure 1. Due to the hierarchical structure of large synthetic fiber ropes, the core and strands are not homogeneous, and are themselves formed from constitutive elements, see Part I. However, at the rope level, the strands and core may be considered as homogeneous, provided that their behavior takes into account their components (constitutive element). It is in this sense that, in this work, we use the wire for the strand.

The axial behavior of such a structure exhibits coupling between tension and torsion due to the helical design of the wires. Thus, the overall behavior can be expressed as:

$$\begin{Bmatrix} F_z \\ M_z \end{Bmatrix} = \begin{bmatrix} k_{\varepsilon\varepsilon} & k_{\varepsilon\theta} \\ k_{\theta\varepsilon} & k_{\theta\theta} \end{bmatrix} \begin{Bmatrix} u_{z,z} \\ \theta_{z,z} \end{Bmatrix} \qquad (1)$$

where $u_{z,z}$ denotes the overall axial strain, $\theta_{z,z}$ the twist angle per unit length, F_z the axial force and M_z the torque. The four stiffness matrix components $k_{\varepsilon\varepsilon}$, $k_{\theta\theta}$, $k_{\theta\varepsilon}$ and $k_{\varepsilon\theta}$ are pure tensile, torsion and coupling terms respectively. Moreover, the stiffness matrix should be symmetric, as can be shown from Betti's reciprocal theorem.

3. Earlier models

This work is concentrated on 1+6 structures in which, in contrast to multilayered structures, the bending moments and torque in individual components should be considered. Several analytical models are available to predict the mechanical behavior of 1+6 metallic structures subjected to axial loads, based on a knowledge of the component material behavior and geometry of the structure. The first approaches only incorporate effects associated with tension, the bending and torsion stiffness of the wires being neglected. Such analyses have been performed by Hruska (1951; 1952; 1953) and by Knapp (1975) for a rigid core. More recent and complex analytical models are based on beam theory assumptions: the behavior of wires is described using Love's curved beam equations. Following this approach, Machida and Durelli (1973) have studied the effects of the bending and torsion stiffness of individual

wires on the cable stiffness matrix. Knapp (1979) studied the effect of variations in core radius. This approach, primarily devoted to soft core cables, can also be applied to more rigid core structures. Costello and Philips (1976) presented a general non-linear theory for a layer of helical wound wires without core, which included the effects of radius and helix angle variations (Poisson's ratio effect). This formulation leads to a set of non-linear equations. A more recent paper by Philips and Costello (1985) presents a solution of the same theory applied to wire rope with internal wire rope cores. Kumar and Cochran (1987) have developed a linearized form of this theory, leading to a closed-form expression for axial stiffness coefficients. This model, was later extended by Kumar and Botsis (2001) to obtain the analytical expression for the maximum contact stresses induced in the multilayered strands with metallic wire core. Huang (1978) studied the contact mode conditions (radial or lateral) for 1+6 cable. Local contact deformation is neglected whilst the Poisson's ratio effect is included. It is found that radial contact seems to be prevailing case, even when no initial gap exists between wires in the layers. Utting and Jones (1987a, 1987b) have extended the model of Costello et al. to include wire flattening (contact deformation) and friction effects. The results show that friction and wire flattening have very little effect on estimates of the global cable response.

Sathikh et al. (1996) presented a closed form symmetric linear elastic model for a cable with a rigid core, using discrete thin rod theory. In this model only core-to-wire contact, the wire tension, twist and bending together have been taken into account. Recently, Costello (1997) presented a linearized theory including the effects of curvature and twist variations. Finally, Labrosse (1998) presented a new analytical approach to predict the overall behavior of 1+6 cables subjected to bending, tension and torsion. In this model, Poisson's ratio effect is neglected while relative motions between core and wires are considered.

Elata et al. (2004) presented a new model for simulating the mechanical behavior of a

wire rope with an independent wire rope core under axial loads. In contrast with previous models that consider the effective response of wound strands, this model considers the complete double-helix configuration of individual wires within the wound strand and directly relates the wire level stress to the overall load applied at the rope level. Bending and torsion stiffness of the individual wires are neglected. Therefore, the accuracy of this model increases when the number of wires in the wire rope increases.

Another approach for multi-layered structures consists in modeling each layer as an equivalent orthotropic sheet developed by Hobbs and Raoof (1982), Raoof and Hobbs (1988). The same approach also consists of replacing each layer with a cylinder of orthotropic, transversely isotropic material (Blouin and Cardou (1989), Jolicoeur and Cardou (1994; 1996), Crossley et al. (2003a ; 2003b)). Such homogenization approaches can be applied when the number of wires in the layer is important, but this is not the case for 1+6 structures.

For all the models mentioned above, the material is considered isotropic, homogeneous and the local behavior of wires and core doesn't exhibit coupling between tension and torsion phenomena.

As indicated in Part I of this paper (see section 3), different models are available for the analysis of fiber ropes ((Leech et al., 1993); (Rungamornrat et al., 2002); (Beltran et al., 2003); (Beltran and Williamson, 2004)) and are implemented in a computer program.

4. Present 1+6 model

Several closed-form formulations have been presented to predict the behavior of 1+6 metallic cables while there are few models for synthetic fiber ropes. In addition, all fiber rope models available are implemented in computer programs (not closed-form model). So we decided to develop a closed-form formulation for synthetic fiber ropes as an extension of an existing model of metallic cables. The comparison of different existing models (1+6 metallic

cables: (Hruska (1951; 1952; 1953); Machida and Durelli (1973); McConnell and Zemeke (1982); Kumar and Cochran (1987); Sathikh et al. (1996); Costello (1997); Labrosse (1998)) with the results of a 3D finite element model has been performed elsewhere by Ghoreishi (2005). The results demonstrated that, generally, the models selected, except Hruska's model (Hruska, 1953), yield very similar results for the usual practical values of lay angle ($\alpha \leq 15°$). In this paper, Labrosse's model has been chosen as a base model because it has a closed-form and symmetric stiffness matrix and the relative motions between core and the wires are considered. Also, this model has the potential to study the friction phenomena between the core and wires, (even if this is not considered in this work due to simplifying assumptions).

The initial Labrosse's model (Labrosse, 1998) which is based on the following hypotheses is developed :

Only the static behavior of structure is addressed;

Displacement and strain are assumed to be small. For a metallic cable, Velinsky (1985) has shown that the results from linear and nonlinear theories are very close in the usual practical load range;

The wires are made of a homogeneous, isotropic and linearly elastic material;

For each wire, a section initially normal to the wire centerline remains plane and normal after deformation;

Poisson's ratio effect and contact deformation are neglected. Utting and Jones (1987a; 1987b) demonstrated that in axial loading, the results are nearly unchanged when the Poisson's ratio and wire flattening are taken into account. This approximation is well established for metallic ropes, and is supposed to be valid also for fiber ropes, even if change in cross sectional area due to contact stresses may arise for such structures which are transversely soft;

Outside wires do not touch each other, which is often a design criterion so as to minimize the friction effect. Moreover, Huang (1978) has shown that core-wires contact seems to be the

prevailing case, even when no initial gap exists between wires in the layers;

Friction effects are neglected. Several authors Utting and Jones (1987a), Leech et al. (1993), Nawrocki (1997) and Ghoreishi et al. (2004) have noted that friction has very little effect on the global cable behavior under axial loads.

In addition, to extend this model to apply to the fiber ropes, the following modification assumptions are made:

Only the axial loading is addressed. The transverse displacements of the cable axis are zero;

Bending stiffness for the core and wires are neglected. This assumption is felt to be reasonable for synthetic fiber components;

The wires are supposed homogeneous at the rope level that are made of an elastic material with a coupling behavior between traction and torsion. This anisotropy appears from the construction effect (no material effect). Indeed, it is the results of twisting various components (yarn, assembled yarn) into a further component.

4.1 Geometry description

Let us consider a 1+6 structure, as indicated in figure 2, in which core and wires are homogenous with a circular cross section. It should be noted that this geometry, usually represents the 1+6 metallic cables. We suppose that the real geometry of fiber ropes, as illustrated in figure 1, can be approximated by this geometry (figure 2) at the rope level.

The geometry is characterized by the core radius R_c, the wires radius R_w, and the lay angle α measured with respect to the cable *z*-axis. The wires centerline is then a helical curve of radius R_h:

$$R_h = R_c + R_w \tag{2}$$

It can be noted that the wire cross-sections are elliptical in the plane perpendicular to

the structure z-axis (see figure 2). Therefore, the pitch length denoted by *P* can be calculated using the following expression:

$$P = \frac{2\pi R_h}{\tan\alpha} \qquad (3)$$

4.2 Displacement field

As shown in figure 3, the centerline of a helical wire forms a helix of radius R_h and lay angle α. Let G^i be a point of a centerline of wire *i* (i runs from 1 to 6 for the wires), its coordinates in the global Cartesian coordinate system $R_0(O,\vec{X},\vec{Y},\vec{Z})$ are defined as follows:

$$\begin{cases} x_{G^i} = R_h \cos(\phi^i) \\ y_{G^i} = R_h \sin(\phi^i) \qquad i = 1...6 \\ z_{G^i} = R_h \dfrac{\phi^i}{\tan\alpha} \end{cases} \qquad (4)$$

where ϕ^i is the polar angle, see figure 3 a). The vectors $\vec{t^i}$, $\vec{n^i}$ and $\vec{b^i}$ are tangent, normal and binormal unit vectors along the helix and their components in R_0 are

$$\left\{\vec{t^i}\right\} = \begin{Bmatrix} -\sin\alpha\sin(\phi^i) \\ \sin\alpha\cos(\phi^i) \\ \cos\alpha \end{Bmatrix}, \quad \left\{\vec{n^i}\right\} = \begin{Bmatrix} -\cos(\phi^i) \\ -\sin(\phi^i) \\ 0 \end{Bmatrix}, \quad \left\{\vec{b^i}\right\} = \begin{Bmatrix} \cos\alpha\sin(\phi^i) \\ -\cos\alpha\cos(\phi^i) \\ \sin\alpha \end{Bmatrix} \qquad (5)$$

that define the local coordinate system $R_i(G^i,\vec{t^i},\vec{n^i},\vec{b^i})$, see figure 3 b).

Let us consider a wire section of center G^i, the displacement field of an arbitrary point M^i, see figure 3 c), according to the classical curved beam theory, can be expressed as follows:

$$\overrightarrow{u_{M^i}} = \overrightarrow{u_{G^i}} + \vec{\theta^i} \times \overrightarrow{G^i M^i} \qquad \mathbf{(6)}$$

where $\overrightarrow{u_{G^i}}$ and $\vec{\theta^i}$ represent the displacement vector at G^i and the rotation vector of the cross

section *i*, respectively, and their components in R_0 are

$$\left\{\overrightarrow{u_{G^i}}\right\}=\begin{Bmatrix}u_x^i(l)\\u_y^i(l)\\u_z^i(l)\end{Bmatrix} \text{ and } \left\{\overrightarrow{\theta^i}\right\}=\begin{Bmatrix}\theta_x^i(l)\\\theta_y^i(l)\\\theta_z^i(l)\end{Bmatrix} \qquad (7)$$

where *l* is the length of the component.

To transform the displacement vector $\overrightarrow{u_{G^i}}$ and the rotation vector $\overrightarrow{\theta^i}$ from global coordinate system R_0 into the local coordinate system R_i, the following relations are used

$$\begin{cases}u_j = a_{jk}\ u_k\\ \theta_j = a_{jk}\ \theta_k\end{cases} \qquad (8)$$

where a_{jk} denote the direction cosines given by:

$$[a]=\begin{bmatrix}-\sin\alpha\sin(\phi^i) & \sin\alpha\cos(\phi^i) & \cos\alpha\\ -\cos(\phi^i) & -\sin(\phi^i) & 0\\ \cos\alpha\sin(\phi^i) & -\cos\alpha\cos(\phi^i) & \sin\alpha\end{bmatrix} \qquad (9)$$

performing the matrix multiplication, displacement components of arbitrary point $M^i\ (0,\xi^i,\eta^i)$, in the local coordinate system $R_i(G^i,\vec{t^i},\vec{n^i},\vec{b^i})$, can be defined as:

$$\left\{\overrightarrow{u_{M^i}}\right\}=\begin{Bmatrix}-u_x^i(l)\sin\alpha\sin(\phi^i)+u_y^i(l)\sin\alpha\cos(\phi^i)+u_z^i(l)\cos\alpha-\eta^i[\theta_x^i(l)\cos(\phi^i)+\theta_y^i(l)\sin(\phi^i)]\\ -\xi^i[\theta_x^i(l)\cos\alpha\sin(\phi^i)-\theta_y^i(l)\cos\alpha\cos(\phi^i)+\theta_z^i(l)\sin\alpha]\\ -u_x^i(l)\cos(\phi^i)-u_y^i(l)\sin(\phi^i)-\eta^i[-\theta_x^i(l)\sin\alpha\sin(\phi^i)+\theta_y^i(l)\sin\alpha\cos(\phi^i)+\theta_z^i(l)\cos\alpha]\\ u_x^i(l)\cos\alpha\sin(\phi^i)-u_y^i(l)\cos\alpha\cos(\phi^i)+u_z^i(l)\sin\alpha\\ +\xi^i[-\theta_x^i(l)\sin\alpha\sin(\phi^i)+\theta_y^i(l)\sin\alpha\cos(\phi^i)+\theta_z^i(l)\cos\alpha]\end{Bmatrix} \qquad (10)$$

The straight core can be considered as a particular case of a helical wire ($\alpha=0$) and for axial loading, its centerline displacement vector can be given by:

$$\begin{cases} u_x^{6+1}(l) = u_y^{6+1}(l) = \theta_x^{6+1}(l) = \theta_y^{6+1}(l) = 0, \\ u_z^{6+1}(l) = u_z, \\ \theta_z^{6+1}(l) = \theta_z. \end{cases} \qquad (11)$$

where superscript *6+1* is referred to the core.

For the moment, the wires and core are modeled independently and displacement field of the whole section of the structure are described by $(6\times 6)+2$, i.e. 38 parameters.

4.3 Contact conditions

In order to reduce the kinematics parameters and to simplify the general form of the displacement field above, core-wires contact (relative motions between core and wires) will be studied.

As shown in figure 4, the contact line between core and wires is also an helical curve of radius R_c and lay angle α' where $\alpha' = Arc\tan(\frac{R_c}{R_h}\tan\alpha)$. The relative motions on the contact line, in the contact point C which is relating to the helical contact line, will be expressed as

$$\begin{cases} \overrightarrow{u_c^{R^i}} = \overrightarrow{u_{c^i}} - \overrightarrow{u_{c^{6+1}}} \\ \overrightarrow{\theta^{R^i}} = \overrightarrow{\theta^i} - \overrightarrow{\theta^{6+1}} \end{cases} \qquad \text{where } C^i \in \text{wire } i \text{ and } C^{6+1} \in \text{core} \qquad (12)$$

where $\overrightarrow{u_c^{R^i}}$ and $\overrightarrow{\theta^{R^i}}$ are the relative translation vector at C and the relative rotation vector between core and wire, respectively.

A new local coordinate system $R_C(C,\overrightarrow{t^i},\overrightarrow{n^i},\overrightarrow{b^i})$ is defined at the contact point C, see figure 4 a). We note that $\overrightarrow{n^i} = \overrightarrow{n^i}$, $\overrightarrow{G^iC^i} = R_w\overrightarrow{n^i}$ and $\overrightarrow{G^{6+1}C^{6+1}} = -R_C\overrightarrow{n^i}$.

The relative translations in the plane (b',t'), $\overrightarrow{u_c^{R^i}}\cdot\overrightarrow{t^i}$ and $\overrightarrow{u_c^{R^i}}\cdot\overrightarrow{b^i}$, represent the sliding, and the relative translation in the direction n' describes relative normal displacement. Rolling and

pivoting are the relative rotations along t' and n', respectively. The relative motion along b' describes relative binormal rotation.

As indicated in figure 4 c), the permanent contact between core and wires leads to the following conditions:

$$\begin{cases} \overrightarrow{u_c^{R^i}} \cdot \overrightarrow{n^{i'}} = 0 \\ \overrightarrow{\theta^{R^i}} \cdot \overrightarrow{b^{i'}} = 0 \end{cases} \qquad (13)$$

The real behavior is bounded by two extreme cases; sliding without friction or no-sliding. As indicated by several authors, Utting and Jones (1987a), Leech et al. (1993), Nawrocki (1997) and Ghoreishi et al. (2004) and Cartraud et Messager (2006), the friction effects on the global cable behavior, subjected to axial loads, are negligible, so, the no-sliding case is considered here or:

$$\begin{cases} \overrightarrow{u_c^{R^i}} \cdot \overrightarrow{t^{i'}} = 0 \\ \overrightarrow{u_c^{R^i}} \cdot \overrightarrow{b^{i'}} = 0 \end{cases} \qquad (14)$$

Nawrocki and Labrosse (2000), using numerical examples, have shown that rolling plays no significant role in the global cable behavior under axial loads. Therefore, it can be supposed to be null,

$$\overrightarrow{\theta^{R^i}} \cdot \overrightarrow{t^{i'}} = 0 \qquad (15)$$

consequently the driving interwire motion under axial loads appears to be only pivoting, $\theta_n^{\ i}(l) = \overrightarrow{\theta^{R^i}} \cdot \overrightarrow{n^{i'}}$.

Using of contact condition hypotheses written previously and making certain mathematical simplifications, allow to reduce the initial number of parameters. The details of these simplifications are available elsewhere (Ghoreishi, 2005) and will not be presented here. Finally, it turns out that the displacement vector of the helical wire centerline can be

expressed as a function of global cable displacement, (u_z, θ_z), and pivoting, $\theta_n{}^i$. One obtains :

$$\begin{cases} u_x^i(l) = R_h \theta_z \sin(\phi^i), \\ u_y^i(l) = R_h \theta_z \cos(\phi^i), \\ u_z^i(l) = u_z, \\ \theta_x^i(l) = -\theta_n^i \cos(\phi^i), \\ \theta_y^i(l) = -\theta_n^i \sin(\phi^i), \\ \theta_z^i(l) = \theta_z. \end{cases} \qquad (16)$$

substituting (16) into the expression (10), the displacement field of an arbitrary point, M^i, on the helical wire section *i* can be expressed in the local coordinate system, $R_i(G^i, \vec{t^i}, \vec{n^i}, \vec{b^i})$, as

$$\left\{\overrightarrow{u_{M^i}}\right\} = \begin{Bmatrix} u_z \cos\alpha + \eta^i \theta_n^i - (\xi^i - R_h)\theta_z \sin\alpha \\ -\eta^i \theta_z \cos\alpha \\ u_z \sin\alpha + (\xi^i - R_h)\theta_z \cos\alpha \end{Bmatrix} \qquad (17)$$

we obtain that in a given section *i*, the kinematics of the section are now described by the 2 degrees of freedom of the structure axis (global displacement) and the 6 relative rotations (pivoting) between the core and wires.

It's recalled that for the core, the kinematics involve only the 2 degrees of freedom of the structure axis, see (10), (11).

4.4 Strain field

Then, the strains can be expressed in terms of the displacement components at point M^i. In the same theoretical framework, the linearized Green strain tensor at point M^i is given by:

$$\varepsilon_{jk}^i = \frac{1}{2}(u_{M^i j,k} + u_{M^i k,j}) \qquad (18)$$

finally, strain tensor components of wire *i*, in the local coordinate system $R_i(G^i, \vec{t^i}, \vec{n^i}, \vec{b^i})$, become

$$\begin{cases} \varepsilon_{tt}^{i} = \dfrac{1}{1-\xi^{i}\,\kappa'}\left(u_{z,z}\cos^{2}\alpha + \eta^{i}\,\theta_{n,z}^{i}\cos\alpha - \xi^{i}\,\theta_{n}^{i}\,\tau - (\xi^{i}-R_{h})\,\theta_{z,z}\cos\alpha\sin\alpha\right), \\ \varepsilon_{nn}^{i} = \varepsilon_{bb}^{i} = \gamma_{nb}^{i} = 0, \\ \gamma_{nt}^{i} = \dfrac{\eta^{i}}{1-\xi^{i}\,\kappa'}\left(-\theta_{z,z}\cos^{2}\alpha + \kappa'\,\theta_{n}^{i}\right) \\ \gamma_{bt}^{i} = \dfrac{1}{1-\xi^{i}\,\kappa'}\left(u_{z,z}\cos\alpha\sin\alpha + (1-\xi^{i}\,\kappa')\theta_{n}^{i} + (\xi^{i}-R_{h})\,\theta_{z,z}\cos^{2}\alpha\right) \end{cases} \qquad (19)$$

where k' and τ represent the curvature and the twist in each wire that, for a circular helix, are given by

$$\begin{cases} k' = \dfrac{\sin^{2}\alpha}{R_{h}} \\ \tau = \dfrac{\sin\alpha\cos\alpha}{R_{h}} \end{cases} \qquad (20)$$

For a given circular cross section under axial loads, in the local coordinate system, twist angle per unit length, $\theta_{t,t}$, is constant (independent of η^{i} and ξ^{i}) and the torsional strains $\gamma^{i}{}_{nt}$ and $\gamma^{i}{}_{bt}$ assumed to increase linearly from zero at the center to a maximum at the external surface of the wire (vary linearly with $\theta_{t,t}$). Consequently, torsional strains at an arbitrary point M^{i} are expressed by

$$\begin{cases} \gamma_{nt}^{i} = -\eta^{i}\,\theta_{t,t}^{i} \\ \gamma_{bt}^{i} = \xi^{i}\,\theta_{t,t}^{i} \end{cases} \qquad (21)$$

while knowing that $\theta_{t,t}$ is constant we obtain

$$\frac{\gamma_{nt}^{i}}{\eta^{i}} + \frac{\gamma_{bt}^{i}}{\xi^{i}} = 0 \qquad (22)$$

then, using equations $(19)_{3\text{-}4}$, the pivoting, θ_{n}^{i}, is found to be:

$$\theta_{n}^{i} = -u_{z,z}\cos\alpha\sin\alpha + R_{h}\cos^{2}\alpha\,\theta_{z,z} \qquad (23)$$

substituting (23) and (20) into the expression (19), we obtain the axial strains of the wire *i* centerline ($\eta^i = \xi^i = 0$) as follows

$$\begin{cases} \varepsilon_{tt}^i = u_{z,z} \cos^2\alpha + R_h\, \theta_{z,z} \cos\alpha \sin\alpha, \\ \theta_{t,t}^i = u_{z,z} \dfrac{\cos\alpha \sin^3\alpha}{R_h} + \theta_{z,z} \cos^4\alpha \end{cases} \qquad (24)$$

It should be noted that the equation (24) was established previously by Sathikh et al. (1996), using Ramsey's theory (1988, 1990) and by Labrosse (1998) using the free pivoting condition between core and the wires, confirming the correctness of the strain field solution.

4.5 Global behavior of the 1+6 structure

At this stage, each component is considered as a structure with a coupling behavior between traction and torsion. It means that the bending moments (M_n^i and M_b^i in the directions $\vec{n^i}$ et $\vec{b^i}$) and shear forces of each individual component are ignored.

The behavior of component i can be expressed in the following matrix form:

$$\begin{Bmatrix} F_t^i \\ M_t^i \end{Bmatrix} = \begin{bmatrix} k_{\varepsilon\varepsilon}^w & k_{\varepsilon\theta}^w \\ k_{\theta\varepsilon}^w & k_{\theta\theta}^w \end{bmatrix} \begin{Bmatrix} \varepsilon_{tt}^i \\ \theta_{t,t}^i \end{Bmatrix} \qquad (25)$$

substituting (24) into the expression (25), axial force and torque (in the tangential direction $\vec{t^i}$) carried by component i, are given as follows:

$$\begin{cases} F_t^i = \left[k_{\varepsilon\varepsilon}^w \cos^2\alpha + k_{\varepsilon\theta}^w \cos\alpha \sin^3\alpha / R_h\right] u_{z,z} + \left[k_{\varepsilon\varepsilon}^w\, R_h \cos\alpha \sin\alpha - k_{\varepsilon\theta}^w \cos^4\alpha\right]\theta_{z,z} \\ M_t^i = \left[k_{\theta\varepsilon}^w \cos^2\alpha + k_{\theta\theta}^w \cos\alpha \sin^3\alpha / R_h\right] u_{z,z} + \left[k_{\theta\varepsilon}^w\, R_h \cos\alpha \sin\alpha - k_{\theta\theta}^w \cos^4\alpha\right]\theta_{z,z} \end{cases} \qquad (26)$$

for the core, tangential direction $\vec{t^i}$ is the cable Z-axis, therefore, core behavior is expressed by:

$$\begin{Bmatrix} F_t^c \\ M_t^c \end{Bmatrix} = \begin{bmatrix} k_{\varepsilon\varepsilon}^c & k_{\varepsilon\theta}^c \\ k_{\theta\varepsilon}^c & k_{\theta\theta}^c \end{bmatrix} \begin{Bmatrix} u_{z,z} \\ \theta_{z,z} \end{Bmatrix} \qquad (27)$$

the stiffness coefficients k_{ij}^{w} and k_{ij}^{c} represent the stiffness matrix components of wire and core respectively. It should be noted that these coefficients can be determined either by test on the components or by the use of a model at a lower scale (continuum model, FRM, …), see part I of this paper.

The force and torque applied to the structure are the resultants of all the forces and torques carried by the central core and wires. The behavior of each component is expressed in the local coordinate system, $R_i(G^i,\vec{t^i},\vec{n^i},\vec{b^i})$. Therefore, by projecting on the cable axis, and summing for all the components (wires and core), global force and torque of structure, in the direction of Z-axis, can be found as follows:

$$\begin{cases} F_z = F_t^c + \sum_{i=1}^{6}[F_t^i \cos\alpha], \\ M_z = M_t^c + R_h \sum_{i=1}^{6}[F_t^i \sin\alpha] + \sum_{i=1}^{6}[M_t^i \cos\alpha] \end{cases} \quad (28)$$

finally the global behavior of a 1+6 fibrous structure can be given by following matrix form:

$$\begin{Bmatrix} F_z \\ M_z \end{Bmatrix} = \begin{bmatrix} k_{\varepsilon\varepsilon}^{*} & k_{\varepsilon\theta}^{*} \\ k_{\theta\varepsilon}^{*} & k_{\theta\theta}^{*} \end{bmatrix} \begin{Bmatrix} u_{z,z} \\ \theta_{z,z} \end{Bmatrix} \quad (29)$$

where $k_{\varepsilon\varepsilon}^{*}$, $k_{\varepsilon\theta}^{*}$, $k_{\theta\varepsilon}^{*}$ and $k_{\theta\theta}^{*}$ represent the global stiffness matrix components that are expressed directly in terms of components stiffness matrix and the geometrical parameters of the structure:

$$\begin{cases} k_{\varepsilon\varepsilon}^{*} = k_{\varepsilon\varepsilon}^{c} + 6\left(k_{\varepsilon\varepsilon}^{w} \cos^3\alpha + k_{\varepsilon\theta}^{w} \dfrac{\sin^3\alpha \cos^2\alpha}{R_h} \right) \\ k_{\varepsilon\theta}^{*} = k_{\varepsilon\theta}^{c} + 6\left(k_{\varepsilon\varepsilon}^{w} R_h \sin\alpha \cos^2\alpha + k_{\varepsilon\theta}^{w} \cos^5\alpha \right) \\ k_{\theta\varepsilon}^{*} = k_{\theta\varepsilon}^{c} + 6\left(k_{\varepsilon\varepsilon}^{w} R_h \sin\alpha \cos^2\alpha + k_{\varepsilon\theta}^{w} \sin^4\alpha \cos\alpha + k_{\theta\varepsilon}^{w} \cos^3\alpha \right) \\ k_{\theta\theta}^{*} = k_{\theta\theta}^{c} + 6 R_h \left(k_{\varepsilon\varepsilon}^{w} R_h \sin^2\alpha \cos\alpha + k_{\varepsilon\theta}^{w} \sin\alpha \cos^4\alpha \right) \\ \qquad + 6\left(k_{\theta\varepsilon}^{w} R_h \sin\alpha \cos^2\alpha + k_{\theta\theta}^{w} \cos^5\alpha \right) \end{cases} \quad (30)$$

5. Comparison between models

In this section, the present 1+6 model is used, and the objective is to compare its results to those of Leech's model.

To apply these models, geometrical and mechanical input data are necessary. To compare the stiffness matrix coefficients, calculated by present model and the Leech approach, two fiber ropes are considered, with 25 Ton and 205 Ton failure loads. The construction details for both of them are presented in Appendix A. The geometrical input parameters at the rope level, which are necessary for the present model, are presented in Table 1.

The mechanical input data required, are the core and wire stiffness matrices. They are obtained form Leech's model, starting at the yarn level (the yarn axial stiffness was obtained from experiments, see part I). FRM software is used in two steps to pass successively to assembled yarn and rope. The results are presented in Table 2.

Then, these core and wires stiffness matrices are considered as input data at the next step (rope level). The 1+6 model presented in the previous section is applied. Leech's model is also used with FRM software and wedge geometry option (see figure 6(b) of part 1 of this paper). It should be noted that in FRM software, a layered packing geometry option can be used only for a structure with identical components, but this is not the case here (core and wires are not identical).

Finally, Table 3 provides the results to compare ropes stiffness matrices, as calculated by the theory presented in section 4 above and Leech's model, for the two 25 ton and 205 ton ropes.

Table 3 shows that, as for the multilayered models presented in Part I, both models for 1+6 structure, yield very similar results for the axial stiffness, $k_{\varepsilon\varepsilon}$. There is a small difference for the coupling terms. Only the torsion term results, $k_{\theta\theta}$, are significantly different for two models. This is easily explained by the fact that, for a given outer diameter, the helix radius

considered by Leech's model is greater than those of 1+6 model (in the wedge geometry, the equivalent helix radius is the radius of the center of area of the wedge), see figure 5. An increase in helix radius does not influence the axial stiffness, $k_{\varepsilon\varepsilon}$, but the coupling terms and the torsion term are related to the helix radius in a linear and quadratic form, respectively.

To show which model gives more reliable results (particularly for the torsion term, $k_{\theta\theta}$), it is necessary to be able to compare them to experimental results. However, as will be discussed in the next section torsion tests on fiber ropes are very difficult to perform.

6. Experiments

The principal tests which have been performed to produce data to compare with the predictions presented above are tensile tests. These enabled values of $k_{\varepsilon\varepsilon}$ and $k_{\theta\varepsilon}$ to be determined, as will be described below. It would also have been very interesting to have been able to obtain a value of $k_{\theta\theta}$ but this proved impossible. Two approaches can be used, either introducing a swivel in the tensile loading system and applying a moment, or loading a sample directly on a torsion test frame. Some preliminary trials on small ropes with swivels produced variable results due to friction of the swivel under load. Torsional stiffness of these materials is quite low and great care is needed with measurements. Tests on a torsion test frame were hampered by difficulty in introducing the load through end fittings without affecting the sample stiffness.

Tension tests were performed on 25 and 205 ton break load samples. The former were performed on a 100 ton capacity test frame at IFREMER in Brest, 8 meter long samples were loaded to 50% of the break load. Figure 6 shows the test frame.

In the second, performed on a specially adapted 500 ton test facility at LCPC

(**L**aboratoire **C**entrale des **P**onts des **C**haussées) in Nantes, a 46 meter long sample of a 205 ton break load rope was blocked at one end and loaded in tension by a hydraulic piston at the other. The tensile response as well as the induced moment were measured at loads up to 100 tons. Figure 7 illustrates the 500 ton test facility at LCPC in Nantes.

In both cases the specimens have been loaded using hydraulic pistons and loads were introduced via splices, see figure 7. All the ropes were made with the same aramid fiber grade (Twaron 1000). Construction details for both fiber ropes are given in appendix A, tables A.1 and A.2.

In order to provide reliable results great care is needed during testing, particularly concerning the following points:

- extensometry
- load measurements
- test procedure.

6.1 Extensometry

The extensions were obtained by three independent measuring systems:

- wire transducers clamped to the central section of the cable,
- two digital cameras measuring the movements of markers in the central part of the cable, and
- an LVDT measuring piston displacement.

The first two measure the true strain in the central part of the rope (away from the splices) and give similar results, as shown in Figure 8. The analysis of the digital images is performed using in-house image analysis software. These values allowed the stiffness measurements to be checked using two independent strain values. The piston displacement was recorded but

not used in stiffness determination as it includes splice, end loop and rope displacements.

6.2 Load measurements

For the 25 Ton rope tests at the IFREMER center in Brest a single load cell at the end of the piston was used. This is calibrated annually. For the tests at LCPC tensile loads were measured using two independent load cells, a 300 Ton capacity cell at the end of the piston and a second 100 ton cell at the fixed end. Both were calibrated before and after the test series. The induced moment was measured using a strain gauged torque meter, calibrated before testing.

6.3 Test procedure

The test procedure includes a preliminary bedding-in loading of 5 cycles to 50% of the nominal break load, followed by either loading to failure or cycling. This initial stabilization of the rope removes bedding-in strain but also results in an internal molecular realignment of the fibers. Figure 9 shows examples of strains measured during the bedding-in cycles of a 25 ton and 205 ton break load ropes. It is clear that without a consistent bedding-in procedure significant variations in stiffness can be measured.

All force, moment and extension data were recorded on a PC acquisition system for post-treatment.

6.4 Test results

The global response of ropes can be expressed by equation (1) and all the tests described above were performed in tension with fixed ends loading conditions ($\theta_{z,z} = 0$). This enabled the axial stiffness $k_{\varepsilon\varepsilon}$ and coupling term $k_{\varepsilon\theta}$, to be determined using following equation (31).

$$\begin{cases} k_{\varepsilon\varepsilon} = \dfrac{F_z}{u_{z,z}} \\ k_{\theta\varepsilon} = \dfrac{M_z}{u_{z,z}} \end{cases} \qquad (31)$$

In the load range of interest, the behavior of aramid fiber ropes exhibits a quasi-linear behavior, as shown in figure 9. Thus, the stiffness matrix components can be considered to be constant, and are obtained from a linear curve fitting.

Results for the 25 Ton rope are summarized in Table 4 below.

As shown in table 4 there is some scatter in the results for different samples, due to variations of material properties and splicing. It should be mentioned that several authors have studied the variability effect on the global response of the fibrous structures (Amaniampong and Burgoyne (1995), Chudoba et al. (2006) and Vorechovsky and Chudoba (2006)), but usually there are different sources of variability.

Table 5 shows the results from the tests on the 205 Ton rope, the coupling term being obtained from the torque meter measurements.

7. Test / models comparison

In this section the experimental results will be compared to model predictions. In both ropes studied here, the base component is the yarn, whose mechanical properties are given as input. For predicting the global behavior of ropes, the presented models are applied in 3 steps, see figure 3 of part I of this paper.

For modeling the 25 ton break load rope, first, to pass from yarn to assembled yarns structure, the yarn axial stiffness and the geometrical parameters enable a prediction to be made of the stiffness coefficients of the assembled yarns using the continuum model presented in the part I of this paper; in the second step, the assembled yarns stiffness matrix (determined in the first step) and the geometrical parameters, can be used to determine the

stiffness matrix coefficients of the strands and core using the present 1+6 model (Eq. (30)). Finally, the strands and core stiffness matrix (determined in the second step) and the geometrical parameters, can be used to predict the global behavior of the 25 ton break load fiber rope using again the present 1+6 model (Eq. (30)), and this gives an axial stiffness value of 11.9 10^3 kN.

To model the 205 ton break load rope, in the same way, the continuum model is applied to pass from yarn to assembled yarns as well as from assembled yarns to core and strands. At the rope level, the 1+6 model is applied to pass from core and strands to 205 ton break load rope.

The strands and core stiffness matrices (determined at the previous step) and the geometrical parameters then enable a prediction to be made of the rope global response using the 1+6 model (Eq. (30)), and this gives axial stiffness, $k_{\varepsilon\varepsilon}$, and coupling term, $k_{\theta\varepsilon}$, values of 99.1 10^3 kN and 205 kN.m respectively.

Therefore, the overall rope behavior is obtained using in sequence the two models (continuum and 1+6) presented in the part I and II of this paper.

The ropes were also treated using Leech's model with the FRM software. This has been used in many previous large fibre rope studies and is commercially available. It was therefore taken as a reference here for comparison purposes, rather than comparing results to all the 1+6 models available in the literature, primarily developed for metallic ropes. This model gives results very close to those of the presented models (11.8 10^3 kN, 98.8 10^3 kN and 215 kN.m for axial stiffness of 25 ton rope, axial stiffness and coupling term of 205 ton rope, respectively). The comparison is shown graphically below in Figures 10 and 11 for 25 ton and 205 ton break load fiber ropes, respectively.

The results show that FRM software (Leech's model) and the presented models give results which are within 1 and 5 percent of each other for axial stiffness, $k_{\varepsilon\varepsilon}$, and coupling

term, $k_{\theta\varepsilon}$, respectively. However, the comparison between predictions and test results are not as close, being 17.5% and 15.8% for the tensile stiffness and coupling terms. This difference appears to be small since the ropes are modeled by taking yarn stiffness and then using three models in sequence. At each step there are errors and these accumulate in the final prediction. If we assume that errors at each step are similar the difference between model and test results at each level may only be around 5%. A larger test database would be useful to examine this in more detail. Moreover, both continuum and 1+6 models neglected the diametral contractions, which therefore contribute to overestimate the rope stiffness.

8. Conclusion

A linear elastic model has been developed for the computation of the elastic axial stiffness terms of a fibrous structure, made of six helical strands wrapped around a straight core (1+6 structure). The helical strands are described as Kirchhoff-Love beams, with constitutive material assumed to be homogeneous, anisotropic linear elastic. Considering static axial loads and small usual lay angles (less than 15°), the friction effects and the lateral contraction of the core have been neglected. The developed approach leads to analytical closed-form expressions.

Due to lack of published experimental data, the model has first been compared with an existing model (Leech's model implemented in FRM software) and is found to provide similar results, except with respect to the torsion term, for which there is a significant difference. Then, two transition models, referred to as a continuum model (see Part I) and the 1+6 model, have been used together in sequence to analyze synthetic fiber ropes. The results of the model at each level have been used as input data for the model at the next higher level. Use of this approach from the lowest level (yarn), at which mechanical properties are given as input, to the highest level of the rope determines the rope axial stiffness matrix. Based on this

strategy, the transition models thus developed can be used to analyze synthetic fiber ropes of various complex cross section. As examples, theoretical results, using the present approach, are determined for 25 ton and 205 ton break load fiber ropes. Tests have also been performed on both fiber ropes with 25 ton and 205 ton rupture force, to obtain experimentally the values of stiffness matrix components. Comparison between models and experimental data shows reasonable agreement, particularly given the low level (yarn) of the input material characteristics.

Therefore, the developed model appear to be reliable and useful, requiring less input data than existing models of the literature. Moreover, the final analytical closed-form solutions allow parametric case studies to be run in order to demonstrate construction effects, at each level, on the global response of fiber ropes and can be used as an optimal design tool. Laboratory full scale testing of large ropes being expensive and time consuming, the development of such theoretical models has the potential to significantly reduce the cost and time needed for cable design.

Appendix A

Construction details for two fiber ropes studied here, with 25 ton and 205 ton failure loads, are given in tables A.1 and A.2. It should be mentioned that all the ropes were made with the same aramid fiber grade (Twaron 1000).

Table A.1: Construction details for new 25 ton synthetic fiber rope.

25T cable					
Structure	Constitutive elements	Number of constitutive elements	Assumed arrangement	Pitch length (mm)	Diameter (mm)
25T cable	Core	**1**	**1 layer**	6.555 (RHL)	16.5
	Strand	**6**	**1 layer**		
Core					
Structure	Constitutive elements	Number of constitutive elements	Assumed arrangement	Pitch length (mm)	Diameter (mm)
Core	Assembled yarn	**7**	**2 layers (1+6)**	**18.868** (RHL)	6
Assembled yarn	Yarn	**16**	3 layers (1+5+10)	**-17 (LHL)**	2.0
Yarn (twaron1000)	Fiber	2000	Parallel fibers	0	0.572
Fiber	-----	------	-----	----	**0.012**
Strand					
Structure	Constitutive elements	Number of constitutive elements	Assumed arrangement	Pitch length (mm)	Diameter (mm)
Strand	Assembled yarn	**7**	**2 layers (1+6)**	**-10.870 (LHL)**	5.25
Assembled yarn	Yarn	**12**	2 layers (3+9)	**19 (RHL)**	1.75
Yarn (twaron1000)	Fiber	2000	Parallel fibers	0	0.572
Fiber	-----	------	-----	----	**0.012**

Table A.2: Construction details for new 205 ton synthetic fiber rope.

205T cable					
Structure	Constitutive elements	Number of constitutive elements	Assumed arrangement	Pitch length (mm)	Diameter (mm)
205T cable	Core	**1**	**1 layer**	2 (RHL)	50
	Strand	**6**	**1 layer**		
Core					
Structure	Constitutive elements	Number of constitutive elements	Assumed arrangement	Pitch length (mm)	Diameter (mm)
Core	Assembled yarn	**42**	4 layers (1+6+14+21)	**6.329 (RHL)**	18.2
Assembled yarn	Yarn	**24**	3 layers (3+7+14)	**14 (RHL)**	3.0
Yarn (twaron1000)	Fiber	2000	Parallel fibers	0	0.572
Fiber	-----	------	-----	----	**0.012**
Strand					
Structure	Constitutive elements	Number of constitutive elements	Assumed arrangement	Pitch length (mm)	Diameter (mm)
Strand	Assembled yarn	**42**	4 layers (1+6+14+21)	**-3.636 (LHL)**	15.9
Assembled yarn	Yarn	**18**	3 layers (1+6+11)	**16 (RHL)**	2.65
Yarn (twaron1000)	Fiber	2000	Parallel fibers	0	0.572
Fiber	-----	------	-----	----	**0.012**

References

Amaniampong, G., and Burgoyne, C. J., 1995. Analysis of the tensile strength of parallel-lay ropes and bundles of parallel elements by probability theory. International Journal of Solids and Structures 32 (24), 3573-3588.

Beltran, J. F., Rungamornrat, J., and Williamson, E. B., 2003. Computational model for the analysis of damage ropes. In: Proceedings of The thirteenth International Offshore and Polar Engineering Conference, Honolulu, Hawai, USA.

Beltran, J. F., and Williamson, E. B., 2004. Investigation of the Damage-Dependent Response of Mooring Ropes. In: Proceedings of The Fourteenth International Offshore and Polar Engineering Conference Toulon, France.

Blouin, F., and Cardou, A., 1989. A study of helically reinforced cylinders under axially symmetric loads mathematical modelling. International Journal of Solids and Structures 25 (2), 189-200.

Cartraud, P., and Messager T., 2006. Computational homogenization of periodic beam-like structures. International Journal of Solids and Structures43 (4), 686-696.

Chudoba, R., Vorechovsky, M., and Konrad, M., 2006. Stochastic modeling of multi-filament yarns: I. Random properties within the cross-section and size effect. International Journal of Solids and Structures 43 (3), 413-434.

Costello, G.A., and Philips, JW., 1976. Effective Modulus of twisted wire cables. Journal of the Engineering Mechanics Division, ASCE, 102, 171-181, 1976.

Costello, G.A., 1997. " Theory of wire rope,". 2nd edition, Springer: New York, N.Y.

Crossley, J. A., Spencer A. J. M., and England A. H., 2003. Analytical solutions for bending and flexure of helically reinforced cylinders. International Journal of Solids and Structures 40 (4), 777-806.

Crossley, J. A., England A. H., and Spencer A. J. M., 2003. Bending and flexure of cylindrically monoclinic elastic cylinders. International Journal of Solids and Structures 40 (25), 6999-7013.

Elata, D., Eshkenazy R., and Weiss M. P., 2004. The mechanical behavior of a wire rope with an independent wire rope core. International Journal of Solids and Structures 41 (5), 1157-1172, 2004.

Foster G.P., 2002 "Advantages of fiber rope over wire rope," Journal of industrial textiles 32 (1), 67-75.

FRM, Fibre Rope Modeller, version 1.1.5, 2003. Software development for Tension Technology International Ltd.(TTI).

Ghoreishi, S. R., Messager, T., Cartraud, P., and Davies, P., 2004. Assessment of Cable Models for Synthetic Mooring Lines. In: Proceedings of The Fourteenth International Offshore and Polar Engineering Conference, Toulon, France.

Ghoreishi S. R., 2005. Modélisation analytique et caractérisation expérimentale du comportement de câbles synthétiques. Ph.D. thesis, Ecole Centrale de Nantes, France.

Ghoreishi, S. R., Cartraud, P., and Davies, P., 2006. Analytical modeling of synthetic fiber ropes subjected to axial loads. Part I : A new continuum model for multilayered fibrous structures. Submitted to International Journal of Solids and Structures

Hobbs, R.E., and Raoof, M., 1982. Interwire slippage and fatigue prediction in stranded cables for TLP tethers. Behaviour of Offshore Structures, Hemisphere publishing/McGraw-Hill, New York, Vol 2, 77-99.

Hoppe, L.F.E., 1991. Modeling the static behavior of Dyneema in wire-rope construction. MTS RTM.

Hruska, F. H., 1951. Calculation of stresses in wire ropes. Wire and wire products 26 (9), 766-767.

Hruska, F. H., 1952. Radial forces in wire ropes. Wire and wire products 27 (5), 459-463.

Hruska, F. H., 1953. Tangential forces in wire ropes. Wire and wire products 28 (5), 455-460.

Huang, N.C., 1978. Finite extension of an elastic strand with a core. Journal of Applied Mechanics 45, 852-858.

Jolicoeur, C., and Cardou, A., 1994. An analytical solution for bending of coaxial orthotropic cylinders. Journal of Engineering Mechanics 120 (12), 2556-2574.

Jolicoeur, C., and Cardou, A., 1996. Semicontinuous Mathematical Model For Bending of Multylayered Wire Strands. Journal of engineering Mechanics 122 (7), 643-650.

Knapp, R.H., 1975. Nonlinear Analysis of a Helically Armored Cable With Nonuniform Mechanical Properties in Tension and Torsion. In: proceeding of IEEE/MTS conference of Engineering in the ocean Environment, San Diego, 155-164.

Knapp, R.H., 1979. Derivation of a new stiffness matrix for helically armoured cables considering tension and torsion. International Journal for Numerical Methods in Engineering 14, 515-520.

Kumar, K., and Cochran, Jr JE., 1987. Closed-Form Analysis for Elastic Deformations of Multilayered Strand," ASME J. Applied Mechanics 54, 898-903.

Kumar, K., and Botsis J., 2001. Contact Stresses in Multilayered Strands Under Tension and Torsion. Journal of applied Mechanics 68, 432-440.

Labrosse, M., 1998. Contribution à l'étude du rôle du frottement sur le comportement et la durée de vie des câbles monocouches. PhD thesis, Ecole Centrale de Nantes, France.

Leech C. M., Hearle J. W. S., Overington M. S., and Banfield S. J., 1993. Modelling Tension and torque Properties of Fibre Ropes and Splices. In: Proceeding of the Third International Offshore and Polar Engineering Conference Singapore.

Leech C. M., 2002. The modeling of friction in polymer fibre rope. International Journal of Mechanical Sciences 44, 621-643.

Machida, S, and Durelli, AJ., 1973. Response of a Strand to Axial and Torsional Displacements. Journal of Mechanical Engineering science 15, 241-251.

McConnell, K. G., et Zemeke, W. P., 1982. A Model to Predict the Coupled Axial Torsion Properties of ACSR Electrical Conductors. Journal of Experimental Mechanics 22, 237-244.

Nawrocki, A., 1997. Contribution à la modélisation des câbles monotorons par éléments finis. PhD thesis, Ecole Centrale de Nantes, France.

Nawrocki, A., et Labrosse M., 2000. A finite element model for simple straight wire rope strands. Computers and Structures 77, 345-359.

Philips, J. W., et Costello, G. A., 1985. Analysis of Wire Rope With Internal-Wire-Rope Cores. ASME Journal of Applied Mechanics 52, 510-516.

Ramsey H., 1988. A theory of thin rods with application to helical constituent wires in cables. International Journal of Mechanical Sciences 30 (8), 559-570.

Ramsey H., 1990. Analysis of interwire friction in multilayered cables under uniform extension and twisting. International Journal of Mechanical Sciences 32 (8), 709-716.

Raoof, M., and Hobbs R. E., 1988. Analysis of Multilayered Structural Strands. Journal of engineering Mechanics 114 (7), 1166-1182.

Rungamornrat, J., Beltran, J. F., Williamson, E. B., 2002. Computational Model for Synthetic-Fiber Rope Response. In: Proceeding of fifteenth Engineering Mechanics Conference, ASCE, New York.

Sathikh S., Moorthy M. B. K., et Krishnan M., 1996. A symmetric Linear Elastic Model for Helical Wire Strands under Axisymmetric Loads. Journal of Strain Analysis 31 (5), 389-399.

Utting W. S., and Jones N., 1987. The Response of Wire Rope Strands To Axial Tensile Loads-Part I. Experimental Results and Theoretical Predictions. International Journal of Mechanical Sciences 29 (9), 605-619.

Utting W. S., and Jones N., 1987. The Response of Wire Rope Strands To Axial Tensile Loads-Part II. Comparison of Experimental Results and Theoretical Predictions. International Journal of Mechanical Sciences 29 (9), 621-636.

Velinsky S. A., 1985. General Nonlinear Theory for Complex Wire rope. International Journal of Mechanical Sciences 27, 497-507.

Vorechovsky, M., and Chudoba, R., 2006. Stochastic modeling of multi-filament yarns: II. Random properties over the length and size effect. International Journal of Solids and Structures 43 (3), 435-458.

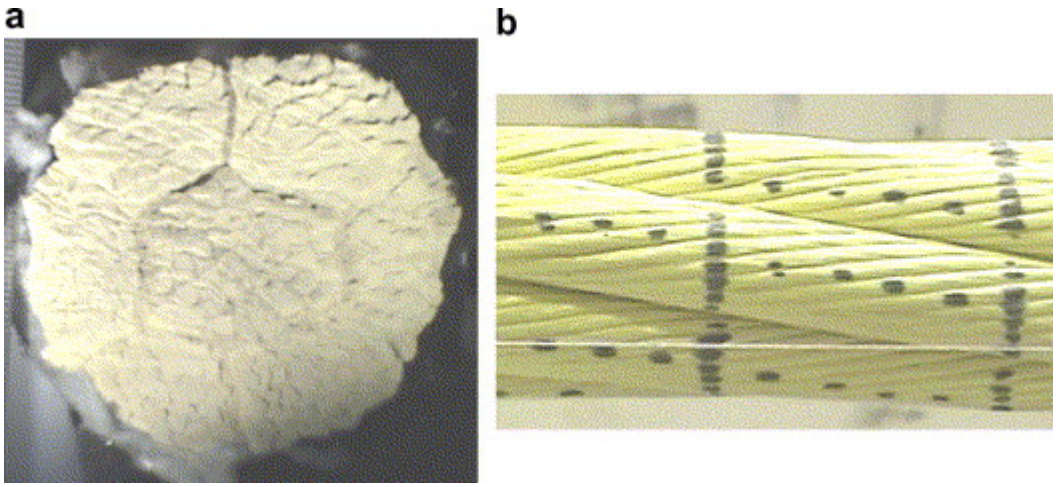

Figure1: 1+6 fiber rope with 205 ton failure loads, a) cross-section, b) side view.

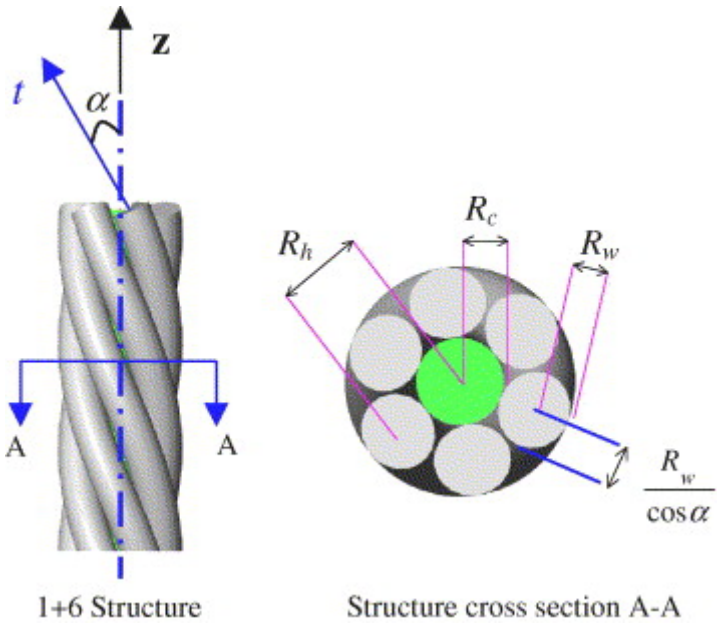

Figure 2: Geometry of a “1+6” structure.

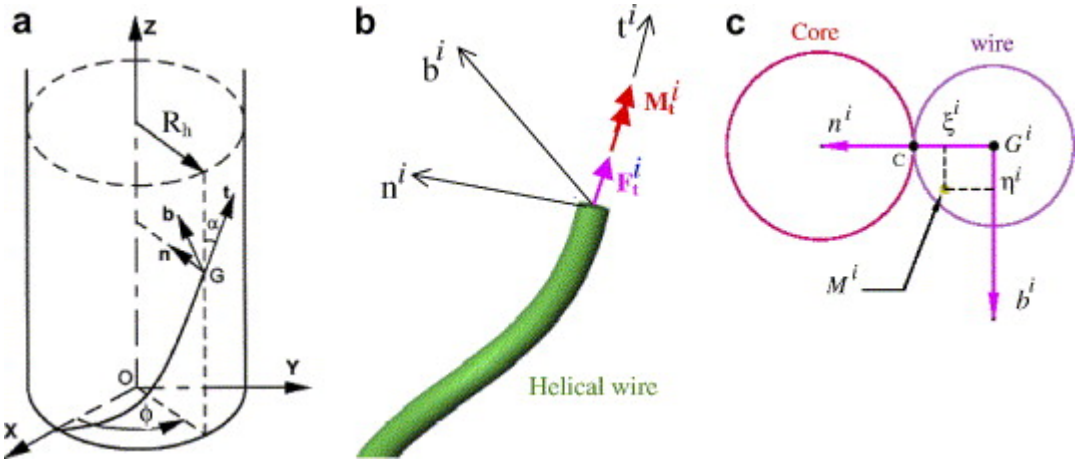

Figure 3: a) centerline of a helical wire, b) axial force and torque in the helical wire, c) local coordinate system.

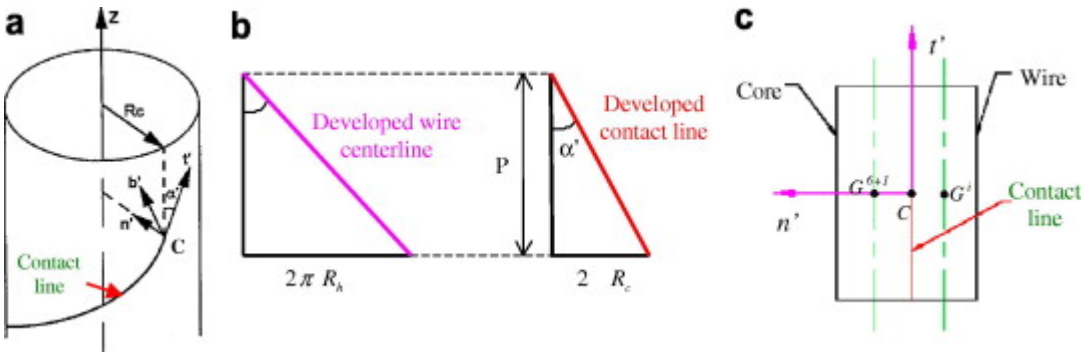

Figure 4: a) local coordinate system $R_C(C,\vec{t^i},\vec{n^i},\vec{b^i})$, b) relation between the lay angle of a helical wire centerline and those of the contact line, c) linear contact core/wire.

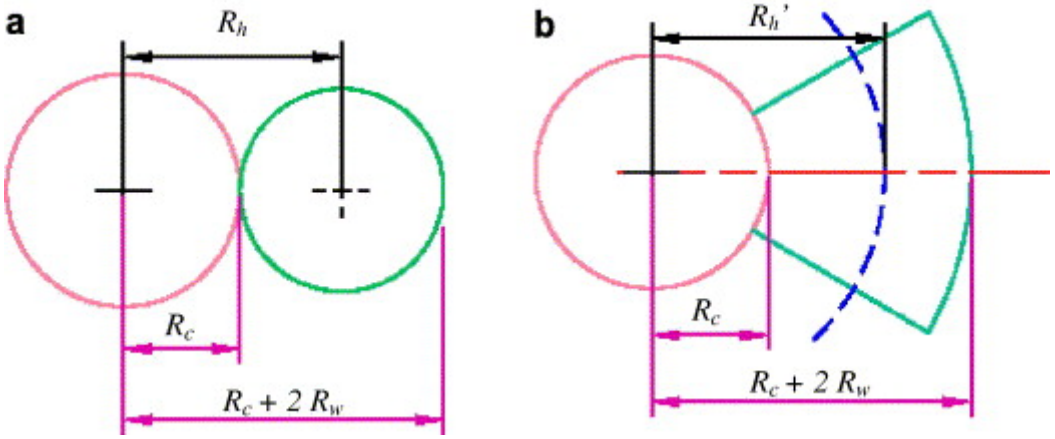

Figure 5: the geometry considered by models, a) present 1+6 model, b) Leech's model (wedge geometry).

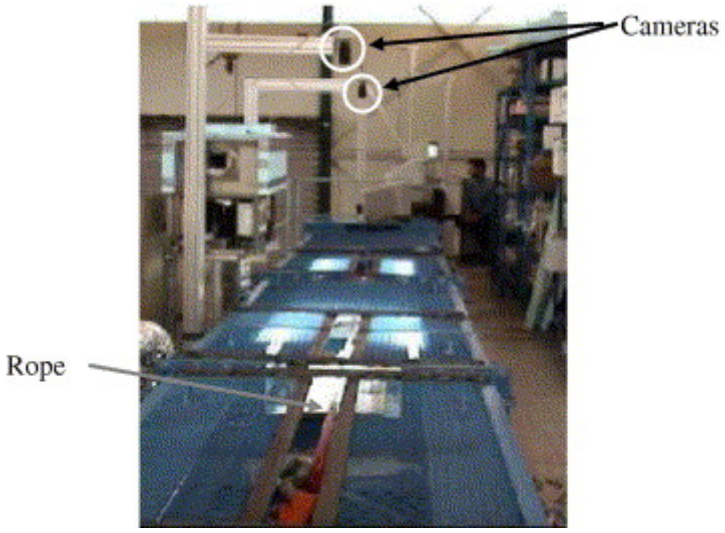

Figure 6: 100 ton capacity test frame, test on 25 ton fiber rope.

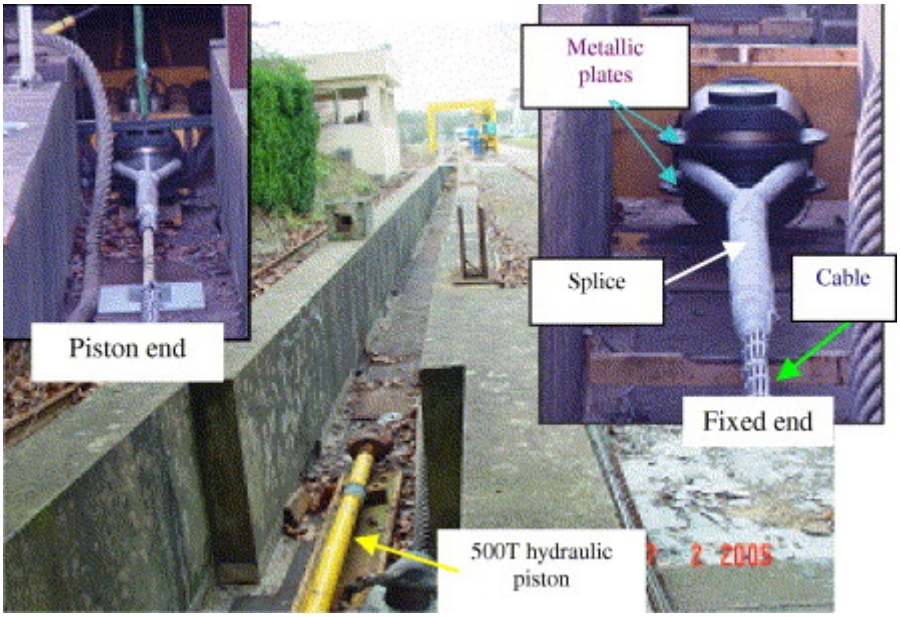

Figure 7: 500 ton test facility at LCPC in Nantes.

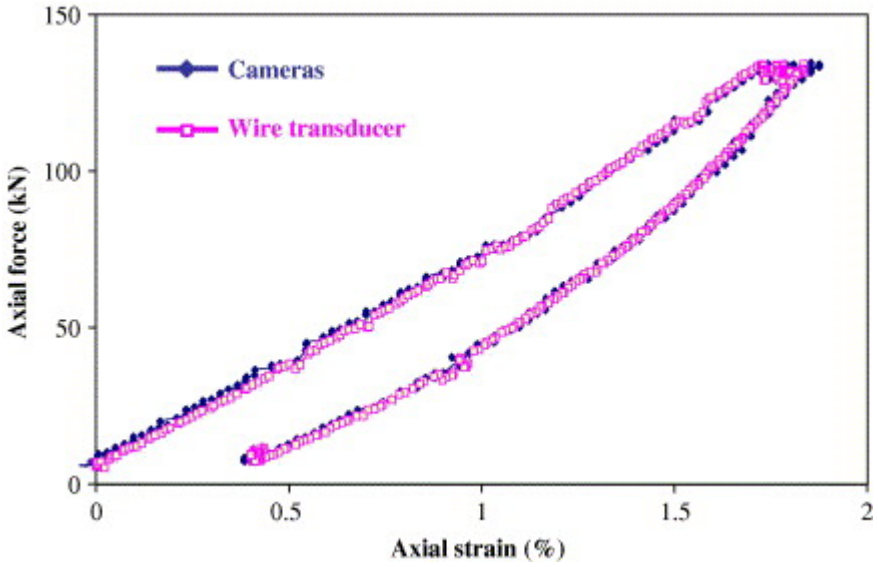

Figure 8 : Comparison between measurements with wire transducer and image analysis system, test on 25 ton break load fiber rope.

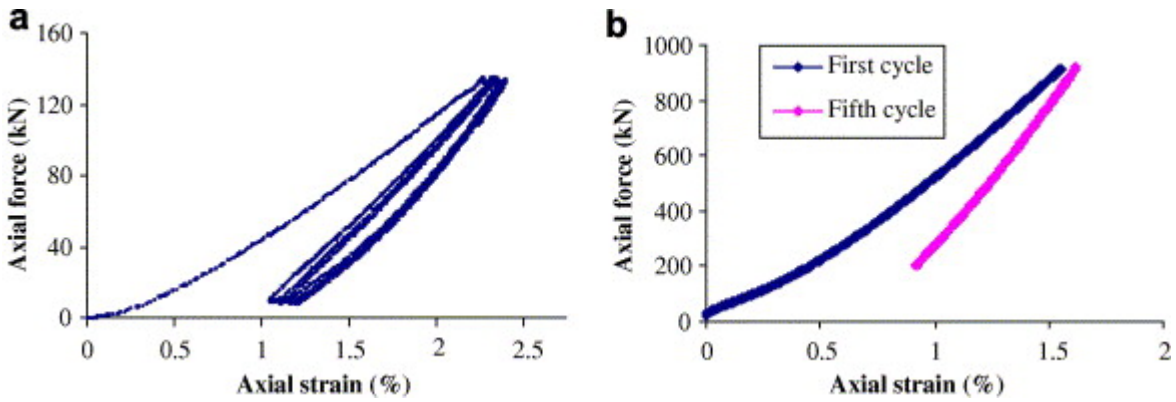

Figure 9: bedding-in cycles, synthetic fiber ropes a) five bedding-in cycles, 25T rope, b) 1st and 5th bedding-in cycles, 205T rope.

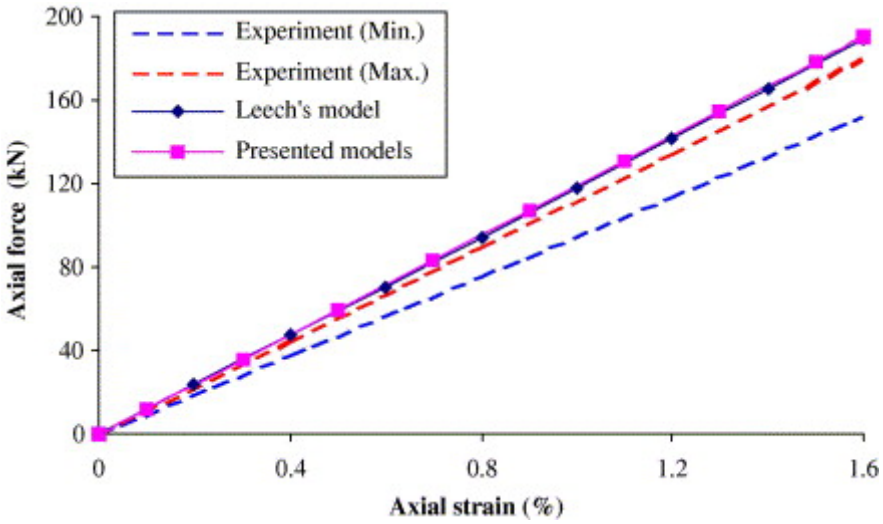

Figure 10: axial stiffness comparison between Leech's model / presented approach / experimental data for 25 ton break load fiber rope.

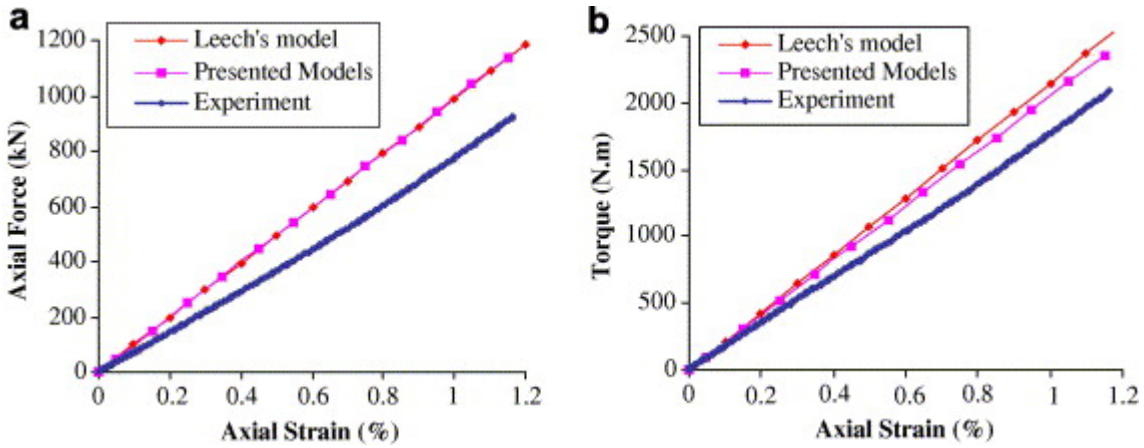

Figure 11: comparison between Leech's model/presented approach/experimental data for 205 ton break load fiber rope, a) axial force versus axial strain, b) induced torque versus axial strain.